Journal of Nuclear Materials 390–391 (2009) 263–266

Contents lists available at ScienceDirect

Journal of Nuclear Materials

journal homepage: www.elsevier.com/locate/jnucmat

Divertor heat load in ITER-like advanced tokamak scenarios on JET

G. Arnoux [a,b,d,*], P. Andrew [a,b], M. Beurskens [a,b], S. Brezinsek [a,c], C.D. Challis [a,b], P. De Vries [a,b], W. Fundamenski [a,b], E. Gauthier [a,d], C. Giroud [a,b], A. Huber [a,c], S. Jachmich [a,e], X. Litaudon [a,d], R.A. Pitts [a,f], F. Rimini [a,d], JET EFDA contributors [1]

[a] JET-EFDA, Culham Science Centre, OX14 3DB, Abingdon, UK
[b] EURATOM/UKAEA Fusion Association, Culham Science Centre, Abingdon, Oxon, OX14 3DB, UK
[c] Forschungszentrum Jülich GmbH, Institut für Plasmaphysik, EURATOM-Assoziation, Trilateral Euregio Cluster, D-52425 Jülich, Germany
[d] Association EURATOM-CEA, CEA/DSM/IRFM, Cadarache 13108 St Paul-Lez-Durance, France
[e] Association "EURATOM-Belgian State" Laboratory for Plasma Physics Koninklijke Militaire scholl – Ecole Royale Militaire Renaissancelaan 30 Avenue de la renaissance, B-1000 Brussels, Belgium
[f] Association EURATOM-Confédération Suisse, Ecole Polytechnique Fédérale de Lausanne (EPFL), CRPP, CH-1015 Lausanne, Switzerland

ARTICLE INFO

PACS:
52.55.Fa
52.55.Rk
52.70.Kz

ABSTRACT

Heat loads on the JET MarkIIHD divertor are measured by IR thermography in high triangularity plasmas with edge conditions of advanced tokamak scenarios (AT). AT scenarios operate at low density ($n_{e,av} < 5 \times 10^{19}$ m^{-3} at JET) to maximise the non inductive current drive, leading to high target temperature ($20 < T_e < 40$ eV), hence high heat loads. Comparisons with a typical baseline inductive scenario ($n_{e,av} \simeq 10 \times 10^{19}$ m^{-3}), show that for similar input power ($\simeq 20$ MW) the outer target heat load is higher by a factor 4 in AT scenario, and is above the limit for the ITER-like wall (ILW). Operating long pulses in AT scenarios in the ILW could then be an issue and heat load reduction using impurity seeding is investigated.

1. Introduction

In a tokamak the divertor is the part of the in-vessel components exposed to the highest heat load. The power handled by the divertor, P_{div}, depends on the input power, P_{in}, and of the amount of radiated power, P_{rad}, such that:

$$P_{div} = P_{in}(1 - \gamma f_{rad}), \quad (1)$$

where $f_{rad} = P_{rad}/P_{in}$. The factor γ is defined such that: $\gamma = 1 - P_{rad,div}/P_{rad}$ where $P_{rad,div}$ is the part of the radiated power contributing to the divertor heating (γ is typically in the range 0.7–0.8 in JET and does not depend on P_{rad} in our data set). The radiative fraction is the key parameter for controlling/reducing P_{div}. The life time of the divertor targets in future fusion devices depends on our capability of controlling their steady state and transient heat load.

The radiated power depends mainly on the density n_e and on the effective charge, Z_{eff}: $P_{rad} \propto n_e^2 Z_{eff}$ [1]. In ITER, f_{rad} is foreseen to be 75% in the baseline (BL) inductive scenario, in order to guarantee a maximum continuous heat load of 10 MW/m^2. Transient heat load due to edge localised modes (ELMs) meet other limits and are discussed in [2–6]. In JET, divertor heat loads have been successfully reduced in inductive scenarios, in ITER-like configuration (plasma triangularity $\delta \simeq 0.4$, elongation, $\kappa \simeq 1.75$), by seeding nitrogen to increase f_{rad} up to 90% [7,8]. This baseline scenario (typically at a plasma current, $I_p = 2.5$ MA, toroidal magnetic field, $B_t = 2.0$ T, safety factor, $q_{95} \simeq 2.6$) operates close to the Greenwald density ($n_{e,av}/n_{e,gwd} = f_{GWD} \simeq 1$), which corresponds to a line averaged density, $n_{e,av}$, of about 10×10^{19} m^{-3}, leading to a natural (without extrinsic impurity seeding) $f_{rad} \simeq 50\%$. The advanced tokamak (AT) scenarios operate at much lower densities ($4 \leqslant n_{e,av} \leqslant 5 \times 10^{19}$ m^{-3}), necessary to achieve high fraction of non-inductive current. This leads to lower natural f_{rad} (15–25%), hence to higher heat load onto the divertor. Fig. 1 shows the heat load profiles measured on the outer divertor target, $q_{\perp}^{outer}$, normalised to P_{in}, for two typical scenarios. The resulting peak heat load is 8 MW/m^2 in the AT scenario and about 2 MW/m^2 in the BL scenario when $P_{in} = 18$ MW and 16 MW, respectively.

The AT scenarios are therefore much more of an issue than BL scenarios for the safety of the future ITER-like wall (ILW) divertor targets, which will be installed in JET in 2009 [9]. A step toward an integrated AT scenario compatible with the ILW has been performed during the JET experimental campaign in 2007 [10]. Dedicated experiments have been conducted in which two types of impurities: neon and nitrogen have been seeded in order to increase f_{rad} from 16% up to 65%. The effect on the confinement

* Corresponding author. Address: EURATOM/UKAEA Fusion Association, Culham Science Centre, Abingdon, Oxon, OX14 3DB, UK.
E-mail address: gilles.arnoux@jet.uk (G. Arnoux).

[1] See Appendix in M.L. Watkins et al., 21st IAEA Fusion Energy Conference, 2006, Chengdu, China.

0022-3115/$ - see front matter © 2009 G. Arnoux. Published by Elsevier B.V. All rights reserved.
doi:10.1016/j.jnucmat.2009.01.094

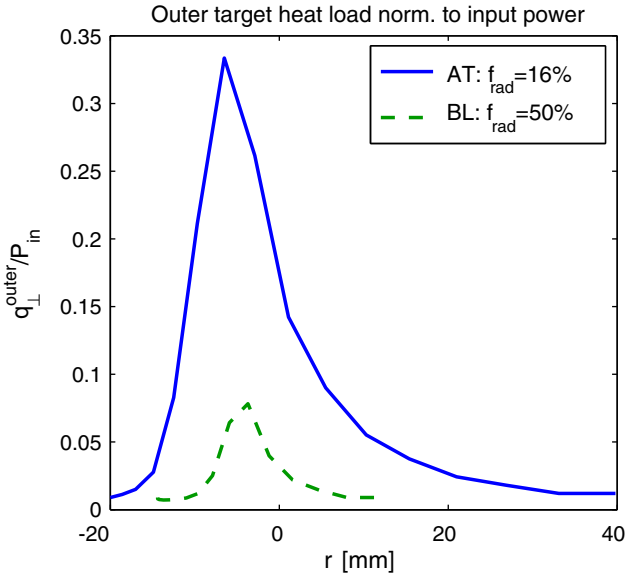

Fig. 1. Outer target heat load profiles (time averaged), $q_{\perp}^{outer}$, normalised to the input power, for an advanced tokamak (AT) scenario where $f_{rad} = 16\%$ and for a typical baseline (BL) scenario where $f_{rad} = 50\%$. The profiles are mapped at the outer mid-plane radius.

and pedestal properties of the plasma are reported in [11] while here we report on the divertor heat load during these experiments. Note that the scenario discussed here has relevant edge conditions but the internal transport barrier (ITB), which is desired in AT scenarios, is not necessarily achieved.

The power conducted onto the divertor is distributed over the inner and outer targets such that $P_{div} = P_{inner} + P_{outer}$. As illustrated in Fig. 2, the JET MarkIIHD divertor is subdivided into eight tiles. For an integrated scenario compatible with the ILW, the outer target (carrying the highest power) must be the tile 5, or the so-called load-bearing septum replacement plate (LBSRP), which will be the only tile made of full tungsten [12]. The power load on that tile should not exceed 7 MW/m^2 for duration of 10 s. Note that higher power can be tolerated for shorter pulse length. The vertical inner target, whether it is tile 1 or 3, will be in carbon fibre composite (CFC) with a tungsten coating [13]. It is expected to carry a third of P_{div} (The power distribution is asymmetric such that $2 < P_{outer}/P_{inner} < 3$ [ELMs] time averaged [14]) but in any case it should not lead to a peak surface temperature higher than 1600 °C to avoid thermal crack of the coating. The two ITER-like magnetic configuration discussed here are shown in Fig. 2, one used for the AT scenario, the other one for the BL scenario.

2. Heat load measurement

The heat load profiles shown in Figs. 1 and 3(a) and (b) are derived from IR images, taken with the wide angle camera installed on JET in 2005 [15,16]. We derive poloidal temperature profiles, $T(s,t)$ (s is a co-ordinate along the cross-section of the divertor) from a narrow toroidal section of the divertor image ($\Delta\phi \simeq 0.5°$). The quality of the profiles is improved compared with those shown in [16] where toroidal averaging over the whole divertor was performed. The resulting [space] spatial resolution, Δs, of 16 mm corresponds to 4 mm at the outer mid-plane radius (considering a flux expansion of 4), which is roughly one power e-folding length ($\lambda_q \simeq 5$ mm [17]) in the scrape-off layer (SOL). A higher [space] spatial resolution would probably lead to narrower profiles with higher peak value.

The heat load profiles, $q_{\perp}^{tile}(s)$, are computed individually for each tile using $T^{tile}(s,t)$ as an input in the finite element code THE-

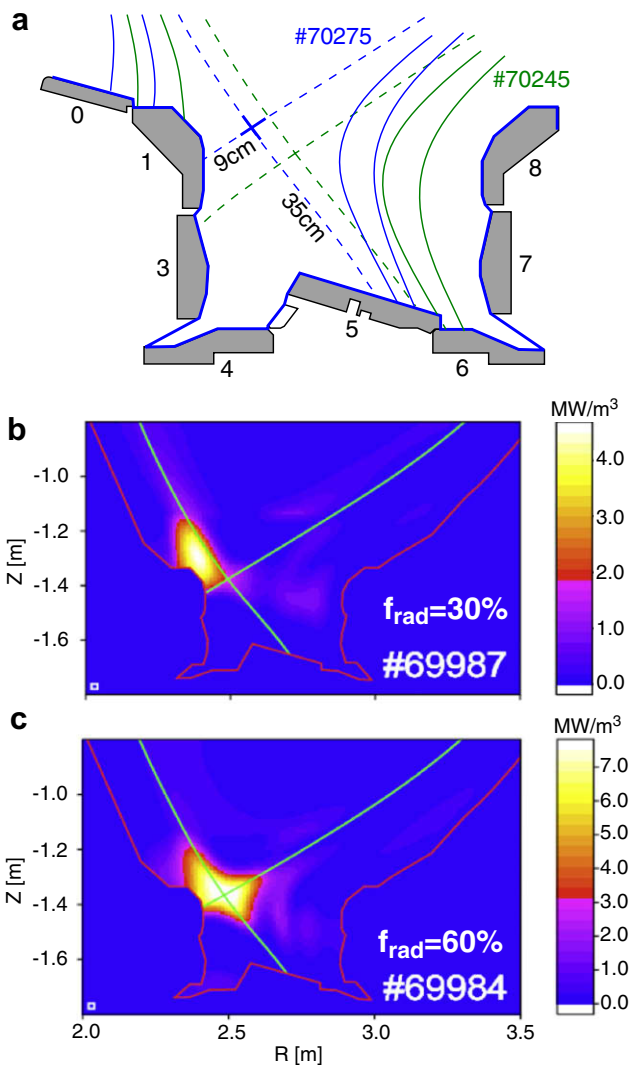

Fig. 2. (a) Schema of the divertor poloidal cross-section superimposed with the magnetic equilibrium of the high δ configuration used in the AT scenarios (blue, #70275) and that of the BL scenario used for comparison (green, #70245). Tomographic reconstruction of bolometer measurements showing the power density radiated in the divertor for (b) $f_{rad} = 30\%$ and (c) $f_{rad} = 60\%$.

ODOR [18,19], which takes into account the surface layer effect (particularly present in the inner divertor [20,16]). The time resolution of the IR diagnostic in that case is $\Delta t = 20$ ms with an exposure time of 60 μs. Therefore the profiles computed for our data set are time averaged over time windows in the range 200 ms–2 s, in which f_{rad} was kept constant.

If we compare the accumulated energy on the inner and outer target, measured by IR, $E_{1,IR}$ and $E_{5,IR}$, with that measured with thermocouples (TC), $E_{1,TC}$ and $E_{5,TC}$, we find that E_{inner} is overestimated ($1.3 < E_{1,IR}/E_{1,TC} < 2.0$) and E_{outer} is underestimated ($0.5 < E_{5,IR}/E_{5,TC} < 1.0$). The reason of this discrepancy is not identified yet, and therefore the power load discussed in the next section are corrected by a factor based on the TC measurements.

3. Heat load reduction

The heat load profiles in Fig. 3 illustrate that indeed increasing f_{rad} decreases the divertor heat load, but this reduction is strongly asymmetric. When f_{rad} increases, P_{outer} is reduced by a factor 2.3 whereas P_{inner} is marginally reduced (about 70% of the initial value). This observation is consistent with the radiation patterns ob-

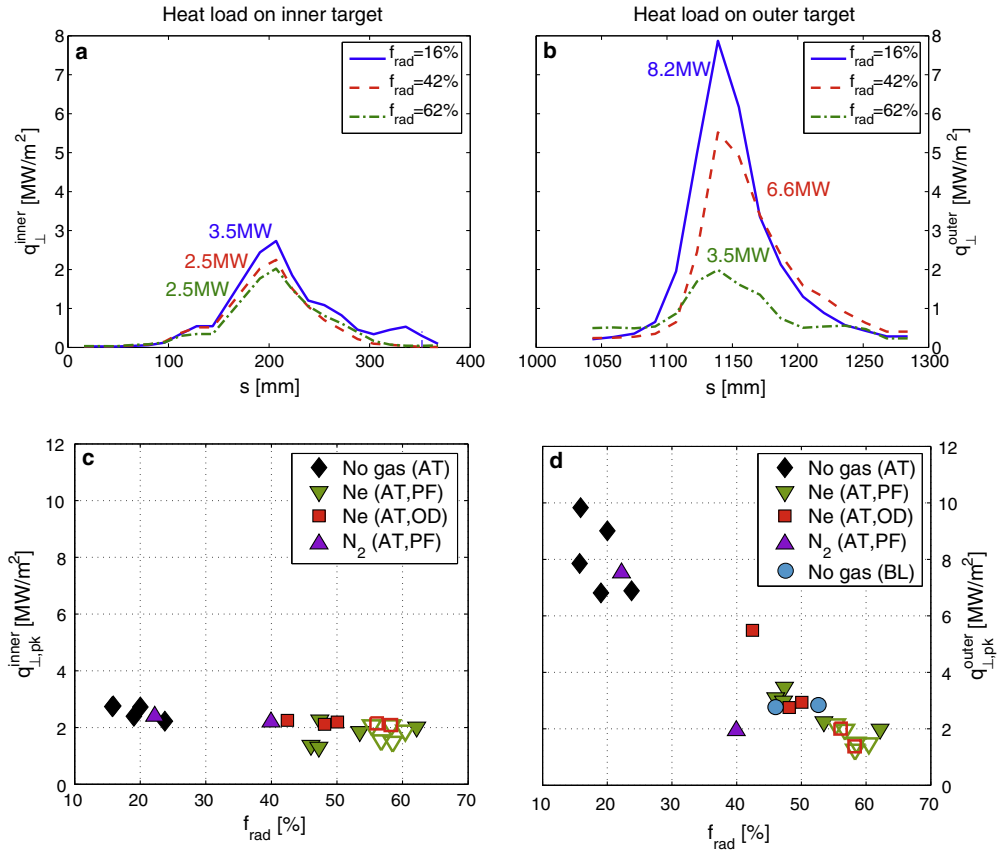

Fig. 3. Inner (a) and outer (b) heat load poloidal profiles for three radiative fractions: 16%, 42% and 62%, achieved with neon seeding. Inner (c) and outer (d) peak heat load as a function of f_{rad} achieved with neon injected from the private flux region (▼) or from the outer divertor (■), or with nitrogen injected from the private flux region (▲). The unseeded AT discharges are indicated by the ◆, and in (d), measurements of unseeded BL scenarios ($f_{rad} \simeq 50\%$) are superimposed (●). The open symbols denote the L-mode plasmas.

tained from tomographic reconstruction of bolometer measurements. As shown in Fig. 2(b), at low f_{rad} the pattern is located above tile 1, and when f_{rad} increases (Fig. 2(c)) the pattern extends around the x-point toward the outer SOL. The proximity of the x-point to the inner target could explain that the impurity seeding cannot cool down the plasma in this region. The electron temperature (inter-ELM) is guessed to remain around 25 eV (langmuir probes coverage for that configuration was not optimal) and therefore the heat load is marginally reduced. A configuration like that used in the BL scenario (Fig. 2(a)), with the inner strike point on tile 3, would probably improve the situation. Unfortunately, the IR diagnostic does not cover that particular tile and we cannot compare.

The peak heat loads measured in unseeded AT discharges show that P_{inner} should not be an issue for the ILW. In Fig. 3(c) (◆), $q^{inner}_{\perp,pk}$ does not exceed 3.5 MW/m^2 for a maximum input power of 24 MW. Such a heat load leads to a surface temperature (semi-infinite model) of 1600 °C after 50 s! For the outer target, Fig. 3(d) (◆) shows that $q^{outer}_{\perp,pk}$ can be up to 10 MW/m^2 ($P_{in} = 24\ MW$) which is above the 7 MW/m^2 required. However this means that with such an input power, shorter pulses should be considered. If the input power is increased at JET up to the foreseen 45 MW, this will become an issue, though the operational density for AT scenarios could be increased as well.

The decrease of $q^{outer}_{\perp,pk}$ achieved with neon seeding (■ and ▼), does not depend on the injection location. Nitrogen seeding (▲) seems to achieve a better reduction at lower f_{rad} (around 40%) though the statistic here is rather poor (note that the fuelling efficiency is much lower with nitrogen). In any case, whether nitrogen or neon was used, detachment seems not to be achieved since (1) the temperature at the outer target remains above 7 eV [10] and (2) no significant change is observed on the shape of the heat load profile. Note that for these discharges, the heat load reduction is at the expense of a degradation of the confinement due to the decrease of the pedestal pressure [11], and even back transition to L-mode is reached (empty symbols in Fig. 3(a) and (b)).

The measurements for the BL scenario (● in Fig. 3(b)) show that when f_{rad} is about 50%, similar heat loads as that in AT scenarios are measured. Although the same heat load is achieved, the physical sputtering, the core pollution and the confinement are expected to be worse in the AT scenario. In the BL scenario, $f_{rad} = 50\%$ is achieved with high density ($n_{e,av} \simeq 10 \times 10^{19}$ m^{-3}) and Z_{eff} seems to remain low ($1 < Z_{eff} < 2$). In AT scenarios, since the density is lower ($4 < n_{e,av} < 5$), it is achieved by injecting impurities yielding to an increase of Z_{eff} (from $Z_{eff} \simeq 2$ at $f_{rad} \simeq 20\%$ to $Z_{eff} \simeq 4$ at $f_{rad} = 50\%$). The introduction of high Z impurities in the divertor region is likely to increase the W sputtering on the outer target, and it is not clear if the plasma will not disrupt due to W accumulation in the core. (In AT scenarios, impurities tend to accumulate in the core due to the ITB.) A clear balance between low target temperature and impurity contents will have to be reached, and the situation can improve at higher density.

4. Conclusion

Divertor heat loads were measured using IR thermography for the first time in plasmas with edge conditions close to that of advanced tokamak scenarios in JET. We have shown that operating AT scenarios in the JET ITER-like wall can be an issue for long discharges with the foreseen nominal input power of 45 MW, especially if the density is not increased. The low density at which AT

scenarios presently operate in JET would require impurity seeding to reduce the heat load. A reduction of the divertor power to the same level as that of a baseline scenario, which operate at higher density, was achieved injecting neon and nitrogen, but at the price of an increase of Z_{eff} and a degradation of the confinement. In addition, the unfavourable divertor configuration of these high δ AT discharges exhibited a strong asymmmetry of the power load reduction. An improvement of the divertor configuration and an increase of the operational density thanks to the higher additional heating power of 45 MW should allow to run AT scenario in the JET ILW but probably for a limited duration.

Acknowledgements

This work was funded jointly by the United Kingdom Engineering and Physical Science Research Council and by the European Committee under the contract of Association between EURATOM and UKAEA. The view and opinions expressed herein do not necessarily reflect those of the European Commission.

References

[1] G.F. Matthews et al., J. Nucl. Mater. 241–243 (1997) 450.
[2] T. Eich et al., J. Nucl. Mater. 390-391 (2009) 760.
[3] W. Fundamenski et al., J. Nucl. Mater. 390–391 (2009) 10.
[4] R.A. Pitts et al., J. Nucl. Mater. 390–391 (2009) 755.
[5] M. Jakubowsky et al., these Proceedings.
[6] A. Kirk et al., J. Nucl. Mater. 390–391 (2009) 727.
[7] P. Monier-Garbet et al., Nucl. Fus. 45 (2005) 1404.
[8] J. Rapp et al., J. Nucl. Mater. 337–339 (2005) 826.
[9] G.F. Matthews et al., Phys. Scr. T128 (2007) 137.
[10] X. Litaudon et al., Plasma Phys. Control Fus. 49 (2007) B529.
[11] M. Beurskens et al., Nucl. Fus. 48 (2008).
[12] Ph. Mertens et al., these Proceedings, doi:10.1016/j.jnucmat.2009.01.253.
[13] G.F. Matthews et al., on behalf of the ITER-like Wall Project Team, these Proceedings, doi:10.1016/j.jnucmat.2009.01.239.
[14] R.A. Pitts et al., J. Nucl. Mater. 337–339 (2005) 146.
[15] E. Gauthier et al., in: Proceedings of the in 24th Symposium on Fusion Technology, Warsaw, Poland, 2006.
[16] G. Arnoux et al., in: Proceedings of the in 34th EPS Conference on Plasma Physic and Controlled Fusion, Warsaw, Poland, 2007.
[17] A. Herrmann et al., J. Nucl. Mater. 313–316 (2003) 759.
[18] A. Herrmann et al., Plasma Phys.Control Fus. 37 (1995) 17.
[19] T. Eich et al., Plasma Phys. Control Fus. 49 (2007) 573.
[20] P. Andrew et al., J. Nucl. Mater. 313–316 (2003) 135.